

Correlations between surface chlorophyll and sea surface height in the tropical Pacific during the 1997–1999 El Niño—Southern Oscillation event

Cara Wilson

NASA Goddard Space Flight Center, GEST Center, Greenbelt, Maryland, USA

David Adamec

NASA Goddard Space Flight Center, Oceans and Ice Branch, Greenbelt, Maryland, USA

Abstract. Correlations between Sea-viewing Wide Field-of-view Sensor (SeaWiFS) surface chlorophyll and TOPEX sea surface height (SSH) are examined in the tropical Pacific (30°S–30°N) using empirical orthogonal function (EOF) analysis both separately and jointly on the two fields. This analysis is done on data from September 1997, the start of data from the SeaWiFS satellite, through December 1999, a time period dominated by the El Niño—Southern Oscillation. Four distinct biological responses are observed. The dominant response is a symmetric off-equatorial chlorophyll increase during La Niña that extends between 2° and 18° latitude from the eastern Pacific to the date line. The chlorophyll mode is tightly correlated to SSH, suggesting that the chlorophyll increase is a result of the shoaling thermocline, which increases the surface nutrient supply. The better known equatorial decrease in chlorophyll during El Niño is seen in a separate EOF mode. Using acoustic Doppler current profiler data from the Tropical Atmosphere-Ocean/Triton array, it is shown that the cessation of the El Niño equatorial chlorophyll minimum is tied to the recommencement of the iron-rich Equatorial Undercurrent which occurs several months prior to the termination of the El Niño. There is an off-equatorial bloom during the peak of the El Niño between 120°W–180°W and 8°N–15°N. This bloom occurs within the area covered by the previously mentioned La Niña bloom, but it is more localized, and its fluctuations appear correlated with changes in the North Equatorial Counter Current. The shoaling thermocline in the western warm pool during El Niño results in a chlorophyll bloom that extends from the Philippines to 155°E between 0°N and 15°N. This bloom terminates in unison with the end of the El Niño when elevated SSH is reestablished in the western basin.

1. Introduction

The surface ocean in the tropical Pacific is nutrient limited, and biological production is strongly coupled to the physical processes that deliver nutrients to the surface, e.g., upwelling, thermocline and mixed layer depth changes, and changes in the current structure. The relative importance of each these processes depends on the regional environmental conditions and ecology. For example, the equatorial Pacific is one of the high nitrate-low chlorophyll regions of the world's oceans where productivity may be controlled by the availability of the micro-nutrient iron [Martin *et al.*, 1991; Coale *et al.*, 1996]. Under normal conditions, wind-driven upwelling along the equator brings iron-rich water from the shallow (~100 m) Equatorial Undercurrent (EUC) to the surface [Coale *et al.*, 1996], supporting relatively high levels of biological productivity [Barber *et al.*, 1996; Landry *et al.*, 1997]. During El Niño a relaxation of the trade winds leads to a reduction or even a reversal of the EUC, cutting off the iron supply to the euphotic zone and limiting production [Chavez *et al.*, 1999]. In contrast, the subtropical gyres are nitrate or phosphate limited [Karl *et al.*,

Copyright 2001 by the American Geophysical Union.

Paper number 2000JC000724.
0148-0227/01/2000JC000724\$09.00

1995], and production there is more linked to changes in the depth of the thermocline and the mixed layer.

Most studies of the physical-biological coupling in the tropical Pacific have been regional, focusing either on the El Niño chlorophyll decrease along the equator [Feldman *et al.*, 1984; Halpern and Feldman, 1994; Barber *et al.*, 1996; Bidigare and Ondrusek, 1996; Chavez *et al.*, 1998] or on the El Niño chlorophyll increase in the western warm pool [Dandonneau, 1986; Leonard and McClain, 1996; Mackey *et al.*, 1997]. Until the launch of the Sea-viewing Wide Field-of-view Sensor (SeaWiFS) satellite most studies relied upon cruise data, which can give only limited temporal and spatial resolution.

The concurrent operation of the TOPEX/Poseidon (T/P) altimeter satellite (launched in August 1992) and the SeaWiFS ocean color satellite (launched in August 1997) provides the first opportunity to analyze large-scale correlations between physical and biological fields of the surface ocean. These sensors observed the sea surface height (SSH) and color anomalies associated with the extremely strong 1997–1998 El Niño and the subsequent La Niña. The El Niño—Southern Oscillation (ENSO) is the largest source of interannual variability for the tropical Pacific, and it affects sea surface temperature, atmospheric pressure gradients, surface winds, ocean currents, thermocline depth, and biological productivity. The magnitude

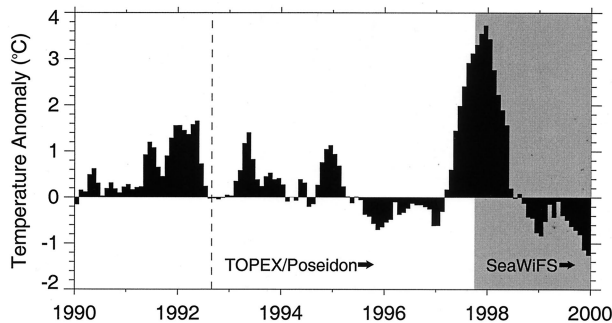


Figure 1. NINO3 index from 1990 to 2000 showing the average sea surface temperature anomaly in the eastern equatorial Pacific (90°W – 150°W by 5°S – 5°N). Generally, indices $>0.5^{\circ}\text{C}$ indicate El Niño events, while indices $<-0.5^{\circ}\text{C}$ indicate La Niña events [Trenberth, 1997]. The time period covered by the SeaWiFS satellite chlorophyll data is shaded and is dominated by the very strong 1997–1998 El Niño and the subsequent La Niña. The start of the TOPEX/Poseidon data in 1992 is indicated by the dashed line.

of the 1997–1998 El Niño can be seen in Figure 1, showing the NINO3 index, the average sea surface temperature anomaly 90°W – 150°W by 5°S – 5°N , during the 1990s. Generally, indices greater/less than 0.5°C / -0.5°C indicate El Niño/La Niña events [Trenberth, 1997]. The 1997–1998 El Niño was the strongest of the century [McPhaden, 1999].

There have been several descriptive analyses of the equatorial chlorophyll decrease during the 1997–1998 El Niño and the subsequent recovery bloom during the La Niña using satellite chlorophyll data in conjunction with physical data [Chavez *et al.*, 1999; Murtugudde *et al.*, 1999; Murakami *et al.*, 2000]. Chavez *et al.* [1999] combine chemical and biological data from the Tropical Atmosphere-Ocean (TAO) moorings and shipboard data with SeaWiFS chlorophyll data to examine the differences in the eastern equatorial Pacific (100°E – 180°E by 10°S – 10°N) between El Niño conditions and normal conditions. Their results highlight the importance of both propagating tropical instability waves and changes in iron flux to the La Niña equatorial bloom. Murtugudde *et al.* [1999] describe the changes in monthly maps of the first year of SeaWiFS chlorophyll in conjunction with T/P SSH data and the results from their ocean general circulation model. In particular, they describe two chlorophyll blooms that occur during El Niño: an off-equatorial bloom between 100°W – 150°W and 10°N – 15°N that they attribute to enhanced entrainment fluxes and lowered SSH height and an equatorial bloom at 165°E at the end of the El Niño caused by the disappearance of the barrier layer due to easterly wind bursts.

The purpose of this study is to examine quantitatively correlations between biological and physical dynamics in the tropical and subtropical Pacific Ocean (30°S – 30°N) during the 1997–1998 El Niño and the subsequent La Niña. Empirical orthogonal functions (EOFs) are used to analyze statistically the temporal and spatial variability of SSH and chlorophyll in the tropical Pacific Ocean. Individual EOF analyses are made for SSH and chlorophyll data and joint EOF analysis is made on both parameters for the time period between September 1997 and December 1999.

2. Data

The SeaWiFS surface chlorophyll *a* data [Hooker and McClain, 2000] from global, 8-day-binned, level 3 standard

mapped images (SMI) are analyzed for the period from September 14, 1997, through December 31, 1999. The SMI data, initially on a $0.09^{\circ} \times 0.09^{\circ}$ grid, is rebinned onto a $1^{\circ} \times 1^{\circ}$ grid. Anomalies are calculated relative to the 27-month average, and the data are deseasoned by subtracting the climatological monthly average values. Finally, the fields are smoothed using a 5° running box mean to reduce small-scale variability. Hence, any variability smaller than ~ 500 km is not part of this analysis.

SSH anomaly data from T/P generation B Merged Geophysical Data Records from September 1997 through December 1999 (T/P cycles 183–268) are used. For internal consistency, only data from the TOPEX altimeter was used. SSH anomalies are calculated relative to the 7-year average from 1993 to 1999, and the resulting fields are averaged along track and optimally interpolated [Bretherton *et al.*, 1976] onto a $1^{\circ} \times 1^{\circ}$ grid temporally centered on the middle day of the 9.9156-day cycle. A more detailed discussion of the initial processing, gridding, and error estimates of the TOPEX data are given by Adamec [1998]. The gridded anomalies are deseasoned by subtracting the monthly averages calculated from the 1993–1999 record. Finally, the SSH data are temporally regridded onto 8-day cycles corresponding to the SeaWiFS data.

3. SSH and Chlorophyll Data

Oceanic plankton ecosystems are generally limited by either light or nutrients (phosphate, nitrate, or micronutrients such as iron), and the limiting factor is impacted by physical factors such as thermocline and mixed layer depth, vertical and horizontal currents, and wind forcing. To understand fully the biophysical coupling, it is necessary to consider how all the factors interact. For example, increased mixing can increase or decrease surface productivity, depending on either the seasonal stratification of the water column [Dandonneau and Goquin, 1984] or on the regionally varying limiting factor [Polovina *et al.*, 1995]. Here the main focus is on SSH, which is an indication of the thermocline depth.

The climatological thermocline depth in the tropical Pacific is shown in Figure 2, with schematic arrows representing the surface currents. The depth of the $\sigma_{\theta} = 25.9$ isopycnal from

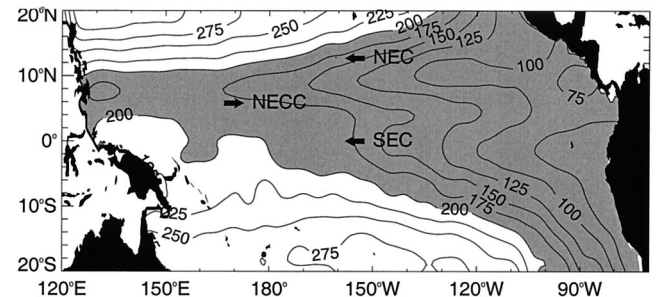


Figure 2. Climatological thermocline depth (in meters) overlaid with schematic arrows representing the surface currents. The depth of the $\sigma_{\theta} = 25.9$ isopycnal from the Levitus data set [Levitus and Boyer, 1994a, 1994b] is used to represent the base of the thermocline, as done by Johnson and McPhaden [1999]. The region where the thermocline depth is <200 m is shaded. The arrows indicate the direction of each current: NEC, North Equatorial Current; NECC, North Equatorial Counter Current; SEC, South Equatorial Current. The Costa Rica dome, an area of strong upwelling in the eastern Pacific, is delineated by the 75-m contour line.

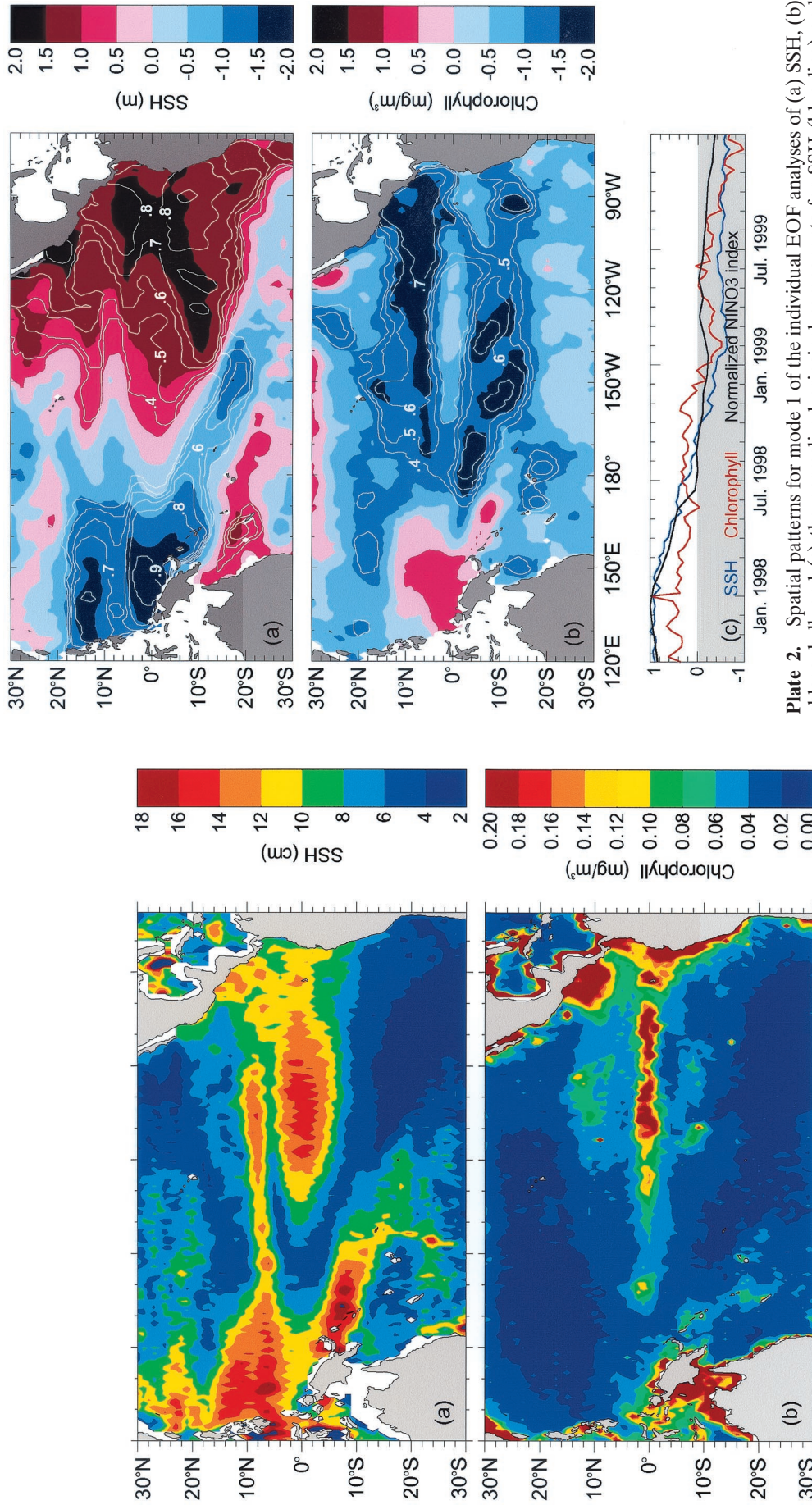


Plate 1. RMS variability for (a) SSH and (b) chlorophyll for the period from September 1997 through December 1999 (seasonal signal removed), where the RMS variability is the square root of the average of the squared variable.

Plate 2. Spatial patterns for mode 1 of the individual EOF analyses of (a) SSH, (b) chlorophyll, and (c) the normalized principal components for SSH (blue line) and chlorophyll (red line) alongside the normalized NINO3 index (black line). This mode accounts for 43% and 26% of the total variance for SSH and chlorophyll, respectively. For a given time and location the sign and magnitude of the spatial component is determined by the product of the principal component at that time and the spatial component at that location. Negative portions of the principal component plots are shaded gray to better distinguish the periods where the principal components change sign. Overlaid on the spatial component maps are contours of the homogeneous correlation, the correlation at each point between the time series of the data and the temporal component. The contour interval is 0.1, and the minimum contour shown is 0.4. Absolute correlations above 0.23 are significant at the 99% confidence level.

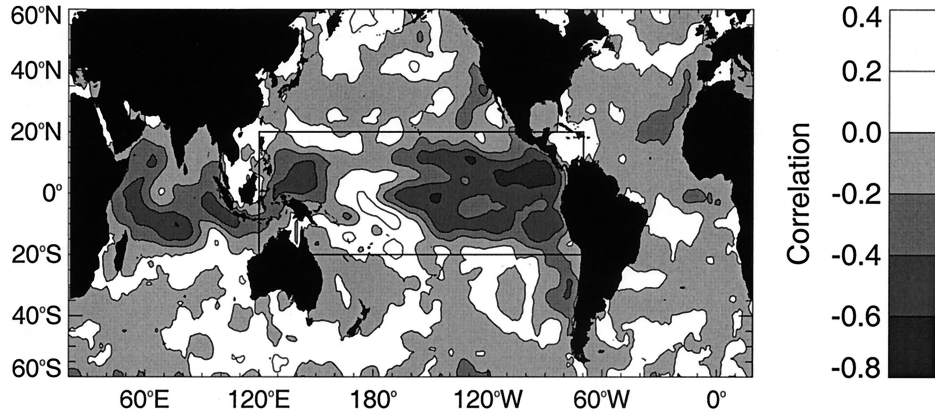


Figure 3. Global correlation map between SSH and chlorophyll. Negative correlations are shaded, while positive correlations are not shaded. The contour interval is 0.2. The strongest correlations are in the Indian and Pacific basins. In the Pacific the largest negative correlations (<-0.4) are seen in the western warm pool and in the eastern cold tongue. Absolute correlations above 0.23 are significant at the 99% confidence level. The boxed area delineates the region shown in Figure 2.

the Levitus data set [Levitus and Boyer, 1994a, 1994b] is used to represent the base of the thermocline, as done by Johnson and McPhaden [1999]. The thermocline is shallowest, less than 100 m, in the eastern Pacific along the equator and along 10°N where wind-driven upwelling occurs. Maximum thermocline depths are found in the western basin where the thermocline is ~ 200 m along the equator and deepens to 250–300 m off the equator. The North Equatorial Current (NEC) flows westward north of 10°N. The eastward flowing North Equatorial Counter Current (NECC) is sandwiched between the thermocline ridges at the equator and at 10°N. From $\sim 2^{\circ}\text{N}$ to $\sim 20^{\circ}\text{S}$ the South Equatorial Current (SEC) flows westward. The strength and zonal location of these currents fluctuates both seasonally and with the ENSO cycle [Wyrtki, 1979; Kessler and Taft, 1987; Taft and Kessler, 1991; Johnson et al., 2000].

To show the regions where SSH and chlorophyll have the largest fluctuations, their root-mean-square (RMS) variabilities are given in Plate 1, where the RMS variability is the square root of the average of the squared variable at each grid point. There are four regions where the SSH variability is high (>10 cm): along the eastern equator (to 160°W) and extending into the Costa Rica dome in the east, in a thin band along 8°N that stretches across the Pacific from the western warm pool to 120°W, in the western warm pool, and in the South Pacific Convergence Zone (SPCZ). The SPCZ is a zone of persistent cloud convection due to atmospheric convergence that stretches southeast from New Guinea to $\sim 120^{\circ}\text{W}$ and $\sim 30^{\circ}\text{S}$ [Vincent, 1994]. High chlorophyll variability ($>0.1 \text{ mg m}^{-3}$) is seen along the eastern equator (100°W–160°W), in the Costa Rica dome and off of the coast of South America, all areas of strong upwelling. The equatorial band of high chlorophyll variability is more tightly confined to the equator (within 2° latitude) than is the band of high SSH variability (within 5° latitude).

For a first-order look at the covariability between SSH and chlorophyll, correlations between the two time series are calculated, and their spatial distribution is shown in Figure 3. A global view is shown to underscore that the SSH-chlorophyll correlations in the tropical Pacific are the highest of anywhere in the ocean; however, the rest of this paper focuses on just the Pacific. The largest correlations ($|r| > 0.4$) occur in the Indian

and Pacific Oceans, with the highest ones ($|r| > 0.6$) being in the Pacific. SSH and chlorophyll are negatively correlated because a larger SSH implies a deeper thermocline that will reduce the availability of nutrients to the euphotic zone for biological uptake. In areas where the thermocline is very deep, thermocline depth changes will have less of an impact on the shallow euphotic zone and on the surface biology. Indeed, within the Pacific, high correlations ($|r| > 0.4$) occur in the western warm pool and in the eastern cold tongue, which are the regions with the shallowest thermocline (shaded area in Figure 2). The highest correlations ($|r| > 0.6$) are seen along the equator near 150°W, in the Costa Rica Dome, and along the 10°N thermocline ridge at 130°W.

3.1. EOF Analysis

The RMS variabilities and the correlation map indicate the spatial variability and covariability of chlorophyll and SSH but cannot provide any details about their temporal variability. To examine simultaneously their spatial and temporal variability, EOF analysis is done. EOF analysis is an efficient method of extracting the dominant temporal and spatial components of variability into a series of orthogonal functions, or statistical modes. While EOF analysis is used routinely in physical oceanography and atmospheric studies, it has been used much less frequently in biological oceanography [e.g., Barale et al., 1986; Mariano et al., 1996; Bartolucci and Luther, 1999]. A brief overview of the method is given below; more thorough discussions on the technique are given by Preisendorfer [1988] and Emery and Thomson [1997]. In EOF analysis a temporally and spatially varying data set, $F(x, t)$, with locations $x = 1, M$ at time $t = 1, N$ is decomposed according to

$$F(x, t) = \sum_{i=1}^N a_i(t) \phi_i(x), \quad (1)$$

where $a_i(t)$ are the principal (temporal) components of the spatial components $\phi_i(x)$. The principal and spatial components are calculated from the eigenvectors and eigenfunctions of the $N \times N$ covariance matrix of the data set. The EOF spatial components represent standing oscillations that vary

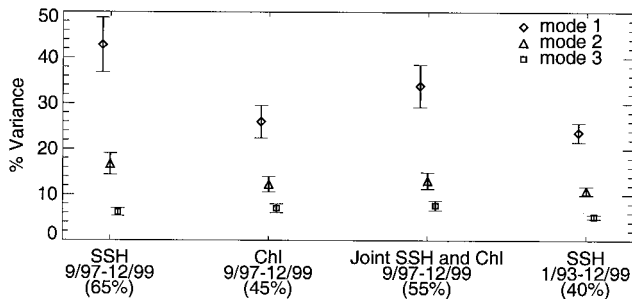


Figure 4. Amount of variance explained by each of the first three modes of the individual SSH and chlorophyll EOF analyses, the joint EOF analyses, and the EOF done on the complete SSH time series. Error bars represent the standard error (1 standard deviation error) for each mode [North *et al.*, 1982]. Modes are statistically different if their error bars do not overlap. The cumulative variance explained by the first three modes is given in parentheses.

according to their principal components. EOF analyses can be done on a single variable or on multiple variables at the same time by constructing the covariance matrix from the variance from the multiple fields normalized by the total variance [Kutzbach, 1967]. In the latter case (joint EOFs) the variables are forced to have the same temporal variability but will have different patterns of spatial variability.

Missing data in the SeaWiFS grids (due to cloud coverage) are not interpolated. Rather, the covariance matrix of the available data is normalized by the number of data used. This technique introduces fewer errors than does interpolating missing data [Davis, 1976; Chelton and Davis, 1982; Emery and Thomson, 1997].

While an EOF analysis will calculate N modes, each with a principal and spatial component, there are typically only a few modes that capture most of the variance. The modes are ranked by the total amount of variance they explain, with the first mode, the dominant mode, explaining the most variance in the data set. Figure 4 shows the percent variance explained by the first three modes (i.e. the modes with the highest percentage of explained variance) for the different EOF analyses presented here, i.e., the EOFs of SSH, chlorophyll, a joint EOF of SSH and chlorophyll, and the SSH EOF using the complete TOPEX time series (1993–1999). The first three modes of the individual EOF analyses of SSH and chlorophyll account for 65% and 45% of the total variance, respectively. The error bars in Figure 4 give the sampling error associated with each mode [North *et al.*, 1982]. Modes are statistically distinct, as are all of the modes presented here, when their error bars do not overlap. EOF analysis is a purely statistical technique, and the derived modes usually, but not necessarily, correspond to physical processes.

3.2. Individual SSH and Chlorophyll EOFs

Plate 2 shows the spatial distributions and principal components for mode 1, which accounts for 43% and 26% of the total variance for SSH and chlorophyll, respectively. The pattern of high SSH in the eastern Pacific and low SSH in the western Pacific (Plate 2a) occurs from September 1997 through August 1998, when the SSH principal component (blue line in Plate 2c) is positive, and switches to low SSH in the east and high SSH in the west after August 1998, when the principal component becomes negative. Overlaid on the spatial component

Table 1. Correlations Between Spatial and Principal Components From Different SSH and Chlorophyll EOFs^a

	Mode 1	Mode 2	Mode 3
<i>Individual SSH and Chlorophyll</i>			
Spatial	-0.47	-0.17	(0.01)
Principal (no lag)	0.84, 0	0.43	(0.12)
Principal, lag	0.84	0.79, -4.0	-0.71, 4.5
	h1/c2 ^b	h2/c3 ^c	h3/c2 ^d
<i>Individual SSH and Chlorophyll</i>			
Spatial	-0.50	-0.47	-0.17
Principal (no lag)	0.48	0.78	0.55
Principal, lag	0.58, 4.5	0.80, 0.3	0.55, 0
	Mode 1	Mode 2	Mode 3
<i>Joint SSH and Chlorophyll</i>			
Spatial	-0.55	-0.45	-0.17
<i>Individual and Joint SSH</i>			
Spatial	0.99	0.98	0.67
Principal (no lag)	0.99	0.95	0.70
Principal, lag	0.99, 0.0	0.95, 0.0	0.74, 0.5
<i>Individual and Joint Chlorophyll</i>			
Spatial	0.95	0.66	0.60
Principal (no lag)	0.90	0.67	0.66
Principal, lag	0.90, 0.0	0.77, -2.7	-0.71, 5.1

^aIndividual modes are EOFs calculated independently on SSH and chlorophyll; joint EOFs are calculated using both variables in one analysis, hence forcing them to have the same temporal variability (see discussion in section 3.1). For the principal components, the correlation with no lag is given as well as the maximum lagged correlation, with the lag given in months. Correlations significant at less than the 99% confidence level are in parentheses. A negative lag indicates that chlorophyll lags SSH or that the individual component lags the joint component.

^bCorrelations of SSH mode 1 with chlorophyll mode 2.

^cCorrelations of SSH mode 2 with chlorophyll mode 3.

^dCorrelations of SSH mode 3 with chlorophyll mode 2.

maps are contours of the homogeneous correlation [Bretherton *et al.*, 1992], which is the correlation between the time series of the data at each point and the principal component in Plate 2. High homogeneous correlations indicate the regions that contribute the most to the temporal variability. Only correlation contours above 0.4 are shown; correlations above 0.23 are significant at the 99% confidence level.

The east-west SSH seesaw seen in Plate 2a is the canonical ENSO thermocline depth oscillation responding to a relaxation of the westerly trade winds [Philander, 1990]. This mode is highly correlated with the NINO3 index (black line in Plate 2c); correlations with the principal components are 0.95 and 0.79 for SSH and chlorophyll, respectively. The high-amplitude negative SSH loadings in the western warm pool and in the SPCZ in the western Pacific reflect the high variability in these areas seen in the RMS field in Plate 1.

Correlations between the spatial and principal components of the SSH and the chlorophyll EOF analyses are given in Table 1. Although the mode 1 principal components for SSH and chlorophyll have a high correlation ($r = 0.84$), their spatial components are markedly different ($r = -0.47$). While elevated SSH oscillates between the eastern and western Pacific, the chlorophyll pattern (Plate 2b) shows reduced chlorophyll throughout most of the Pacific. The small region of elevated chlorophyll in the western Pacific does not signifi-

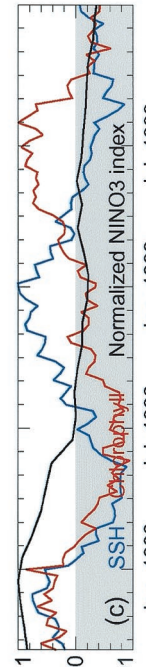
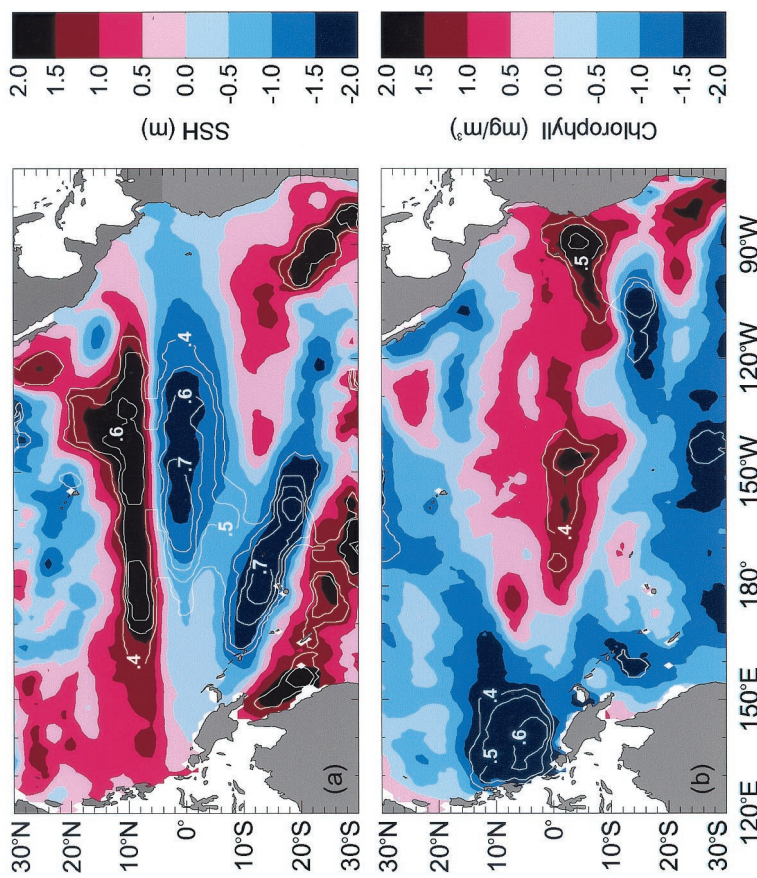
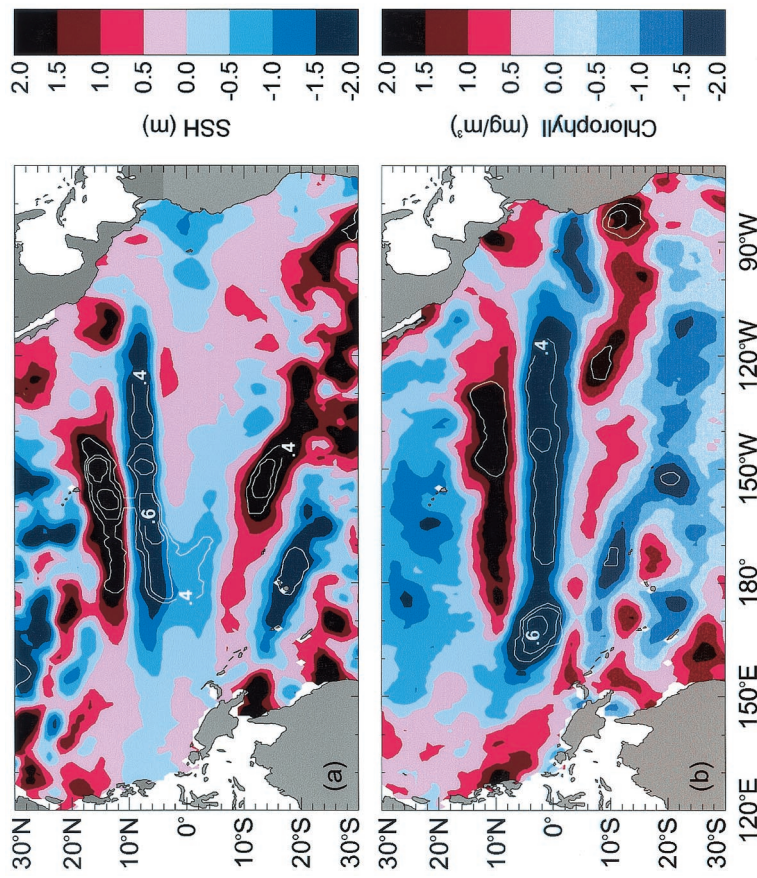


Plate 3. Same as in Plate 2 but for mode 2 which accounts for 16% and 12% of the total variance for SSH and chlorophyll, respectively.

Plate 4. Same as in Plate 2 but for mode 3, which accounts for 6% and 7% of the total variance for SSH and chlorophyll, respectively.

cantly contribute to this mode. The regions of reduced chlorophyll switch to elevated chlorophyll when the principal component changes sign in December 1999, several months after both the change in the SSH principal component and the transition to La Niña conditions. The region of reduced/elevated chlorophyll during El Niño/La Niña extends from the coast of Central and South America to 180° between 18°S and 18°N. However, the chlorophyll spatial loadings are considerably reduced at the equator, and the regions that explain most of the variance lie between 2° and 18° latitude. Most of the area with reduced chlorophyll during the El Niño is within the region of elevated SSH in Plate 2a and within the region where SSH and chlorophyll are correlated in Figure 3. However, the area of reduced chlorophyll extends further west in the EOF modes than does the elevated SSH. At the equator the chlorophyll transition from positive to negative spatial loadings occurs near 160°E, while the SSH transition occurs near the date line. A possible reason for this is that advection is spreading out the chlorophyll bloom.

The deepening of the thermocline throughout the entire eastern and central Pacific during El Niño, seen in the SSH data in Plate 2a, reduces the supply of nutrients and limits chlorophyll production. The large-scale off-equatorial chlorophyll response has not been documented before. While an off-equatorial ENSO-related chlorophyll bloom is discussed by Murtugudde *et al.* [1999], it is a much more localized bloom in the eastern Pacific between 100°W–150°W and 10°N–15°N, while this EOF pattern clearly shows a much larger geographical response between 2° and 18° both north and south of the equator and extending as far west as 180°. Furthermore, Murtugudde *et al.* [1999] describe an off-equatorial chlorophyll bloom during the El Niño, while the EOF mode describes a large-scale off-equatorial chlorophyll decrease during the El Niño and a bloom during La Niña.

While mode 1 does show the chlorophyll changes typically associated with an El Niño, i.e., an equatorial chlorophyll decrease and a bloom in the western warm pool, neither of these regions has very large spatial loadings, and the homogeneous correlations (HCs) are <0.4. Higher HCs delineate the regions where the temporal trend of the data corresponds the best to the principal component for that mode and hence delineate the regions that contribute the most to the mode. In a similar fashion, one can assess what regions dominate during different time periods. For example, to determine if the spatial trends vary between the El Niño and the La Niña, HCs are calculated for two subsets of the time series, between September 1997 and December 1998 and between July 1998 and December 1999. While the El Niño was over by the summer of 1998, these time periods are chosen so that they have similar lengths. The two sets of HCs are shown in Figure 5. There are significant changes between the HC distribution during the El Niño time period (solid contours) and during the La Niña time period (dotted contours). For both chlorophyll and SSH, two regions dominate during the El Niño: a broad area centered in the western warm pool and the region of the cold tongue in the east. The chlorophyll distributions are confined to within 10° of the equator, while the SSH distributions extend farther off the equator and there is a shift in their latitudinal boundaries. In the east the SSH distributions are centered south of the equator between 5°N and 20°S, while the western region is centered north of the equator between 20°N and 5°S. During the La Niña, three regions dominate the SSH distributions: along 10°N and 10°S in the eastern Pacific and in the SPCZ in the

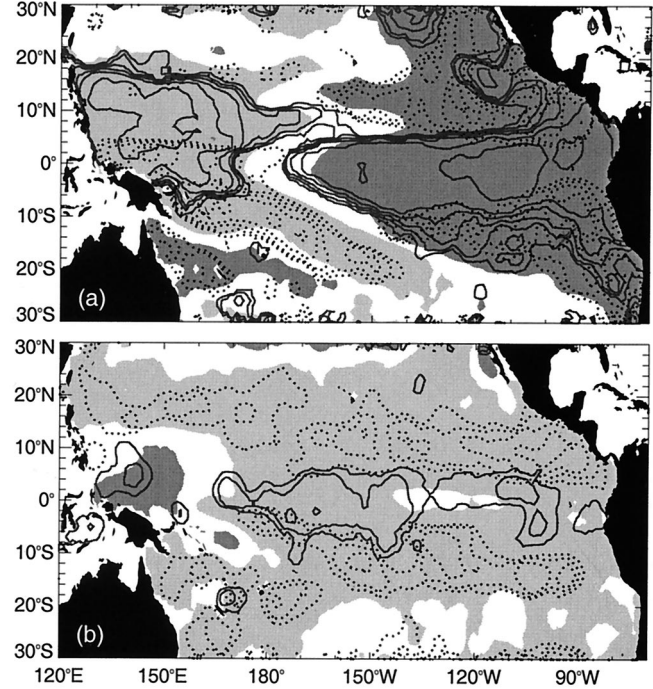


Figure 5. Homogeneous correlations for mode 1 (a) SSH and (b) chlorophyll for the El Niño period (solid contours) and the La Niña period (dotted contours). The El Niño correlation is done using data from September 1997 through December 1998, and the La Niña correlation is done using data from July 1998 through December 1999. While the El Niño was over by the summer of 1998, these time periods are chosen so that they have similar lengths. The contour interval is 0.1, and the minimum contour shown is 0.4. Absolute correlations above 0.3 are significant at the 99% confidence level. Gray regions delineate areas with absolute spatial loadings (from Plate 2) greater than 0.5. Light gray represents negative loadings; dark gray represents positive loadings.

western Pacific. The combination of the El Niño and the La Niña distributions of SSH HCs is virtually identical to the HC distribution in Plate 2a, meaning that all the SSH regions that contribute significantly during either El Niño or La Niña also contribute significantly during the entire time series.

In contrast to the SSH, there are regions in Figure 5b that contribute significantly to the chlorophyll mode during the separate El Niño and La Niña time periods that do not contribute when analyzed over the entire time series. Notably, the dominant contribution during El Niño along the equator region contributes little to the overall mode in Plate 2b. During El Niño, there are HCs of >0.4 along the equator both in the warm pool region of elevated chlorophyll and throughout the eastern and central Pacific region of reduced chlorophyll. During La Niña, HCs of >0.4 are all poleward of 5°, and in the eastern and central Pacific they occur in the same regions as during the entire time series (Plate 2b). These results indicate that the ENSO chlorophyll oscillation shown in EOF mode 1 is driven more by a chlorophyll increase during La Niña than by a chlorophyll decrease during El Niño.

The SSH and chlorophyll HCs in Figure 5 show the equatorial region dominating the variability during the El Niño and show the eastern and central off-equatorial (poleward of 5°) region dominating during La Niña. During the La Niña the regions in the eastern Pacific with high SSH HCs (indicating

reduced SSH) also have high chlorophyll HCs (indicating elevated chlorophyll), with two exceptions: the coastal areas off of Baja California and off of South America where the SSH HCs are >0.4 but the chlorophyll HCs are <0.4 . The southern branch of the chlorophyll HC contours extends farther west, to 170°E , than do the SSH HC contours, which only extend to 150°E , which could be due to advective effects.

Plate 3 shows EOF mode 2, which accounts for 16% and 12% of the total variance for SSH and chlorophyll, respectively. The SSH spatial component is characterized by a band of low SSH spanning the entire basin between 6°N and 10°N when the principal component is positive. Directly south of this band, there is a transition to high SSH that extends down to 10°S and is maximum at the equator. These two areas also have high SSH variability, as seen in Plate 1. There is another area of elevated SSH, associated with the SPCZ, extending southeast from the equator at 150°E to 120°W at 30°S . The principal component is positive during the peak of El Niño and changes sign at the end of February 1998, when the Pacific is past the peak of El Niño but is still experiencing El Niño conditions. The principal component switches again in February 1999, just after the La Niña peak. In contrast to the trend in mode 1, the ENSO cycle produces an apparent 18-month period in mode 2.

This SSH mode can be associated with the variability in the depth of the 10°N thermocline ridge and with the strength of the NECC. The dominant negative loadings lie along the 10°N thermocline ridge (see Figure 2), and when the principal component is positive, as during the El Niño, the thermocline is shallower and the NECC is stronger. This scenario generally agrees with previous studies that have observed a stronger NECC during an El Niño and a weak or absent NECC during a La Niña [Wyrtki, 1979; Kessler and Taft, 1987; Taft and Kessler, 1991; Johnson *et al.*, 2000], although our results suggest that the transition from a strong to a weak NECC occurred at the end of February 1998, still within the El Niño period. However, our results are consistent with conductivity-temperature-depth measurements that indicate that the NECC was strong throughout 1997 (transport $>40 \times 10^6 \text{ m}^3 \text{ s}^{-1}$) and absent during February through July 1998 [Johnson *et al.*, 2000]. Observations show that the NECC was reestablished (transport of $9 \times 10^6 \text{ m}^3 \text{ s}^{-1}$) by September 1998 [Johnson *et al.*, 2000], while the mode 2 principal component SSH changes suggest that this reestablishment occurred in January 1999.

The chlorophyll spatial component for mode 2 (Plate 3b) has negative loadings in a broad region around the central and eastern equatorial Pacific, maximum along the equator, and has positive loadings everywhere else. The areas with the highest HCs (>0.4) are in the western warm pool, which has a chlorophyll bloom during El Niño, and in two patches along the equator in the central Pacific and off the coast of South America, where there is a chlorophyll decrease. The chlorophyll spatial loadings are more similar to those of SSH mode 1 ($r = -0.47$) than to those of SSH mode 2 ($r = -0.17$). The similarity is particularly striking for the chlorophyll bloom west of 155°E , between the equator and 15°N , where SSH mode 2 does not have any high HCs but SSH mode 1 does. Since the EOF analysis is done independently on SSH and chlorophyll, identical mode numbers need not necessarily correspond to one another. The chlorophyll bloom in the western warm pool during the El Niño results from the doming of the thermocline during this time period, as seen in Plate 2a, which brings nutrients to the normally oligotrophic water of the western warm pool. The chlorophyll bloom disappears at the end of

June 1998, coincident with the change in sign of the NINO3 index and 2 months before the change in the SSH principal component (Plate 2c). There is another chlorophyll bloom in this region after July 1999; however, it is uncertain what causes this, as it is not associated with thermocline changes reflected in SSH mode 2.

While separate HCs for the El Niño and La Niña periods were also calculated for this mode, they are not shown as their spatial trends are similar to those in Plate 3. During both El Niño and La Niña the regions around the eastern and central equator, the NECC, and the SPCZ contribute the most to the SSH variability, and these regions also dominate the SSH mode for the entire time series, as seen in Plate 3a. However, for the chlorophyll, there is a change in the dominant regions between the El Niño and the La Niña. The eastern and central equatorial region (to the date line) dominates only during the El Niño, and in that time period a larger area around the equator has high HCs compared to the entire time series. In contrast, the equatorial region does not contribute significantly (HCs of <0.4) during La Niña except in a small region in the western Pacific warm pool. This result is similar to that from mode 1 in that both modes better reflect equatorial chlorophyll changes occurring during El Niño than those occurring during the La Niña.

Plate 4 shows EOF mode 3, which accounts for 6% and 7% of the total variance for SSH and chlorophyll, respectively. Elevated SSH oscillates between two narrow bands north and south of 10°N and two bands near the SPCZ. Chlorophyll is low along the entire equator during the peak of the El Niño, and the HCs are >0.4 across most of the central equator. The mode oscillates to high equatorial chlorophyll in February 1998, 5 months prior to the onset of the La Niña, when strong El Niño conditions still dominate. Of the three EOF modes shown, mode 3 best demonstrates the well-known equatorial chlorophyll decrease during El Niño. Elevated spatial loadings and HCs are more concentrated along the equator than in the two previous modes. Furthermore, in the separate HC analysis for the El Niño and the La Niña time periods (not shown) the equatorial region dominates during both periods, indicating that along the equator this mode is representing well both phases of the ENSO event, whereas in both mode 1 and mode 2 the equatorial region only contributes significantly to the chlorophyll mode during the El Niño time period.

The equatorial chlorophyll variability can be related to changes in the EUC. The equatorial region is iron limited, and productivity is linked to the supply of this micronutrient via the EUC [Barber *et al.*, 1996; Coale *et al.*, 1996; Gordon *et al.*, 1997; Landry *et al.*, 1997]. Levels of iron within the EUC ($0.35 \text{ nmol kg}^{-1}$) are nearly an order of magnitude higher than surface concentrations ($0.05 \text{ nmol kg}^{-1}$) [Coale *et al.*, 1996]. The deepening of the EUC at the start of the 1997–1998 El Niño was coupled with an equatorial chlorophyll decrease [Chavez *et al.*, 1998]. The EUC magnitude is shown in Plate 5 for September 1997 through December 1999 using acoustic Doppler current profiler data from the TAO/Triton array [McPhaden *et al.*, 1998]. Across the Pacific the EUC was absent or weakened during the peak of the El Niño (winter 1998), when the equatorial chlorophyll in mode 3 is low. The sudden reappearance of the EUC in January–February 1998 coincides with the mode 3 oscillation to increased chlorophyll (Plate 4c). A comparison between the maximum velocity, the depth of the maximum velocity, and the chlorophyll principal component (not shown) indicates two regimes: at the beginning of the time series the

Table 2. Correlations Between Principal Component of Chlorophyll Mode 3 (Plate 4) and Maximum Velocity of EUC and Depth of Maximum Velocity^a

Complete Time Series			El Niño		La Niña	
Velocity	Depth		Velocity	Depth	Velocity	Depth
165°E	0.85	-0.75	0.91	-0.85	0.57	-0.76
170°W	(0.05)	-0.36	0.89	-0.83	-0.44	(-0.08)
140°W	(0.03)	-0.33	0.87	-0.89	-0.46	(0.15)
110°W	(-0.23)	(-0.04)	(0.08)	-0.77	-0.40	(0.30)

^aCorrelation was done for the complete time period of overlapping data (September 1997 through the end of the ADCP time series), for the El Niño time period (September 1997 through June 1998), and for the La Niña time period (July 1998 onwards). The length of the record during La Niña is different for each mooring (see Plate 5). The correlation was done using the chlorophyll principal component multiplied by -1, so that a positive value of the principal component indicates higher equatorial chlorophyll. Correlations significant at less than the 99% confidence level are in parentheses.

chlorophyll component is correlated with the depth and strength of the EUC, while at the end of the time series it is not. Correlations between the chlorophyll principal component and the depth and zonal velocity of the EUC are given in Table 2 for the entire time series, for the El Niño period (September 1997 through June 1998), and for the La Niña period (July 1998 onward). Periods with an ill-defined EUC are excluded from the correlation by not using data from late 1997 if the depth of the maximum zonal velocity is >50 or <200 m. Throughout the central and western Pacific, chlorophyll is positively correlated with the EUC velocity and is negatively correlated with the depth of the EUC during the El Niño. In the eastern Pacific, at 110°W, there is no correlation with zonal velocity. Correlations are weaker during the La Niña for both velocity and depth, and many of the correlations have changed sign. Changes in the degree of biophysical coupling with the ENSO cycle have previously been noted [Halpern and Feldman, 1994]. Chlorophyll changes during El Niño could be due to other factors affecting iron flux, such as the strength of local upwelling or temporal changes in the iron levels of the EUC, or they could be due to other factors such as zooplankton grazing, which plays an important role in regulating equatorial chlorophyll levels [Frost and Franzén, 1992; Landry et al., 1997], or the passage of tropical instability waves or equatorial trapped internal waves that have been shown to affect surface chlorophyll [Chavez et al., 1999; Friedrichs and Hofmann, 2001]. However, because of the high-frequency motion of these waves, their effects probably would not show up in our analysis.

The region of negative chlorophyll loadings in Plate 4 at 165°E that is separated from the negative chlorophyll loadings in the central equatorial region by closed HC contours is the area of the bloom discussed by Murtugudde et al. [1999]. The negative loadings represent a bloom when the principal component is negative, which occurs between February and August 1998. Murtugudde et al. [1999] attribute this bloom to easterly wind bursts that reduced the barrier layer in this region. Here we propose that this bloom is caused by the recommencement of the EUC; however, the two explanations are not mutually exclusive, and both could play a role in the equatorial bloom.

Mode 3 (Plate 4) also shows elevated chlorophyll during El Niño in small regions north and south of the equator between 5°N and 15°N in the central and eastern Pacific. This off-equatorial chlorophyll bloom is asymmetric, spanning a larger area in the north than in the south. The southern bloom includes the Marquesas Islands at 140°W, 10°S, which is a region of high productivity due to the island mass effect [Signorini et

al., 1999]. The northern bloom is centered over the 10°N thermocline dome between 120°W and 180°W. The mode 3 chlorophyll spatial and temporal components are better correlated with the mode 2 SSH components than with the mode 3 SSH components. Since the EOFs are run independently on SSH and chlorophyll, identical mode numbers need not necessarily correspond to one another. The spatial and temporal correlations (-0.47 and 0.78, respectively) between SSH mode 2 and chlorophyll mode 3 (h2/c3) are nearly twice as high as the correlations between the mode 2 components or between the mode 3 components. Both SSH mode 2 and chlorophyll mode 3 have sharp transitions between positive and negative spatial loadings across 6°N. The mode 3 chlorophyll bloom occurs where there is simultaneously lower mode 2 SSH, indicating an elevated thermocline/nutricline and a stronger NECC. Unlike the ecosystem at the equator, the ecosystem at 10°N is nitrate limited, and thus biological production is more directly linked to changes in the thermocline depth which affect nitrate availability. This result is consistent with that of Murtugudde et al. [1999], who also described this chlorophyll bloom and attributed it to enhanced entrainment fluxes due to reduced SSH. Similar responses have been observed in this region during other El Niño events. For example, Dymond and Collier [1988] observe an increase in production at 11°N during the 1982–1983 El Niño that they surmise is due to an enhanced NECC flow and the associated shallower thermocline. Fiedler et al. [1992] observe significant changes in the euphotic zone nitrate levels at 10°N associated with the 1987 El Niño.

3.3. Joint SSH and Chlorophyll EOFs

The EOFs shown in section 3.2 were run independently on the SSH and chlorophyll data. Joint EOF analysis was also performed on the two variables to highlight how they covary. In this analysis the EOFs are constructed from the covariance matrix constructed from both variables, and hence they are forced to have the same temporal variability. The first three modes of the joint analysis account for 55% of the total variance. The first mode, explaining 34% of the variance, is the ENSO mode; it is not shown, as its spatial and temporal components are identical to those in Plate 2 (the spatial components of the individual and joint analyses are correlated at 0.99 and 0.95 for SSH and chlorophyll, respectively, and at 0.99 and 0.90 for the principal components; see Table 1).

Mode 2 of the joint analysis is shown in Plate 6 and accounts for 13% of the total variance. The joint spatial and temporal principal components for SSH are virtually identical to those of the individual SSH components for mode 2, having correla-

tions of 0.98 and 0.95, respectively. However, the chlorophyll components differ, having spatial and principal correlations of 0.66 and 0.77, respectively. The spatial components are better correlated for the joint mode than for the individual modes: -0.45 versus -0.17 (see Table 1). The primary difference between the individual and joint spatial modes of the chlorophyll is that the equatorial region dominates more in the joint EOF. In the joint mode, low chlorophyll is more evenly centered along the equator and extends farther west, and the correlations along the equator are higher than in the individual mode. The equatorial band of low chlorophyll corresponds to the region of elevated SSH (deeper thermocline) in Plate 6a. There are patches of low chlorophyll present in the region of the southern branch of high SSH, but it is not a continuous feature as it is in the equatorial region, and the region does not contribute significantly to the mode. The low chlorophyll and high SSH at the equator transition to high chlorophyll and low SSH at the end of February 1998, coincident with the reformation of the EUC (Plate 5). As with the individual EOF analysis where the SSH mode 2 was better correlated with chlorophyll mode 3, the joint chlorophyll mode 2 has a slightly stronger resemblance to the individual mode 3 than to mode 2 because the equatorial region dominates more in the joint chlorophyll mode.

Mode 3 of the joint analysis is shown in Plate 7 and accounts for 8% of the total variance. The overall features of the joint SSH spatial mode are very similar to the individual mode in Plate 4 ($r = 0.67$). The primary differences between the individual and joint spatial modes of the chlorophyll are that most of the positive loadings along the eastern and western boundaries of the Pacific are absent in the joint mode and the regions that contribute the most to the joint mode are more spread out throughout the basin rather than concentrated at the equator as in the individual mode. In the joint mode, positive loadings are confined to the bands in the central Pacific between 5° and 10° south and north of the equator, and these areas do not contribute significantly (HCs of <0.4). The equatorial region in the joint mode, unlike the individual mode, does not contribute very much to the mode nor does it have high HCs, which reflects the stronger representation of the equatorial region in joint mode 2.

Given the dominance of ENSO dynamics during the time of this study (see Figure 1), it would be beneficial to see how these modes behave during quieter periods of the ENSO cycle. While the SeaWiFS record only starts in August 1997, the T/P satellite was launched in August 1992. To put the EOF modes into a larger temporal context, an EOF analysis was done on the 7-year SSH record between January 1993 and December 1999. The principal components for the first 3 modes are shown in Figure 6. The spatial components are not shown, as they are generally similar to those shown in Figure 5 and Plates 2–4. Correlations between the spatial and temporal components of the shorter SSH time series (shown in Figure 5 and Plates 2–4) and the longer time series (Figure 6) are given in Table 3. From Figure 6 it is clear that while modes 2 and 3 are not correlated with the NINO₃ index, they are both obviously impacted by the 1997–1998 El Niño. For all three modes, changes in the principal component between 1993 and 1996 are small compared to the changes between 1997 and 1999. The main point from the longer EOF analysis is that the low-frequency temporal changes seen in all SSH modes of the September 1997 through December 1999 analysis are driven by the 1997–1998 El Niño, and it seems likely that the same

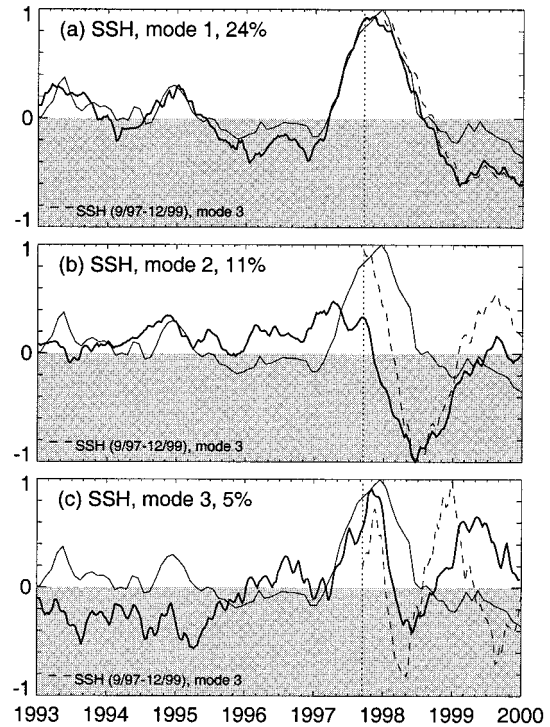


Figure 6. Normalized principal components (thick line) of EOF modes (a) 1, (b) 2, and (c) 3 for the TOPEX SSH record between January 1993 and December 1999. The spatial components are not shown, as they are very similar to those shown in Figure 5 and Plates 2–4. The thin line is the normalized NINO₃ index, and the dashed line is the principal component from the September 1997 through December 1999 analysis. The vertical dotted line indicates the start of the data shown in Figure 5 and Plates 2–4.

would hold true for the patterns observed in the chlorophyll data.

4. Discussion and Conclusions

Not surprisingly, variability in the Pacific during September 1997 through December 1999 is dominated by responses to the strong El Niño of 1997–1998. The different biological responses to the ENSO oscillations arise from a combination of ecological and physical dynamics. The eastern and central equatorial Pacific are iron limited, while the western equatorial Pacific and the subtropical gyres are oligotrophic. Where iron is not limited, changes in the thermocline depth, as reflected in

Table 3. Correlations Between Spatial and Principal Components of Individual SSH EOF Analysis Between September 1997 and December 1999 and Components From EOF Analysis of Data from January 1993 through December 1999^a

	Mode 1	Mode 2	Mode 3
Spatial	0.96	0.76	0.19
Principal (no lag)	0.99	0.90	0.45
Principal, lag	$0.93, -0.3$	$-0.85, -6.5$	

^aFor the principal components, the correlation with no lag is given as well as the maximum lagged correlation, with the lag given in months. All correlations are significant at the 99% confidence level.

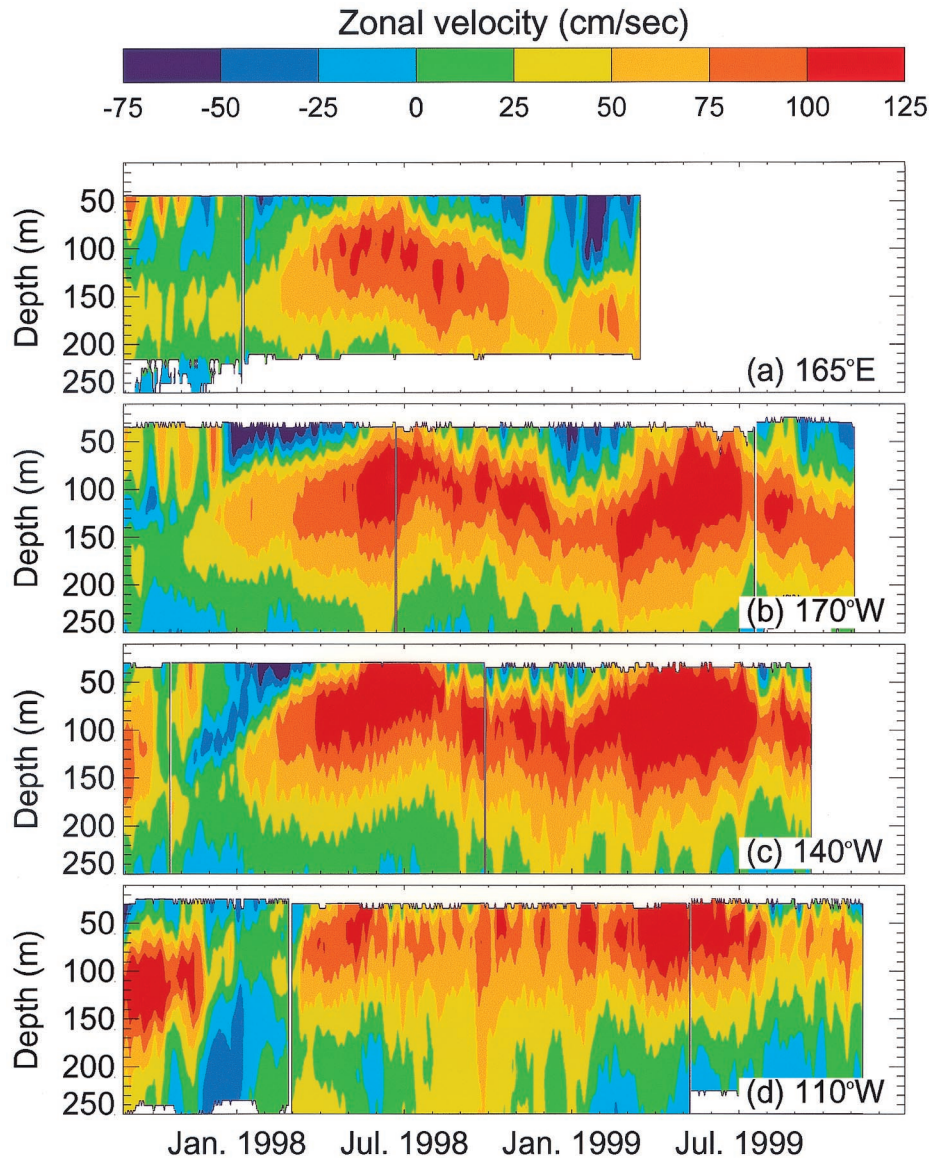


Plate 5. Zonal velocity data from the TAO/Triton equatorial ADCP moorings showing the strength of the eastward EUC from September 1997 through 1999 at (a) 165°E, (b) 170°W, (c) 140°W, and (d) 110°W. Positive velocities are eastward currents. The EUC is weakened or absent during the peak of the El Niño and strengthens suddenly at the beginning of 1998.

the SSH changes, drive chlorophyll variability. The thermocline shoaling in the eastern and central Pacific during La Niña results in a large-scale off-equatorial chlorophyll bloom that extends from the eastern Pacific to the date line between 2° and 18° both north and south of the equator. Similarly, the thermocline rise in the western warm pool during El Niño delivers nutrients to the surface, resulting in a chlorophyll bloom that disappears when the thermocline deepens again at the end of the El Niño. Shoaling of the 10°N thermocline ridge in the eastern Pacific associated with strengthening of the NECC during the peak of the El Niño leads to a localized chlorophyll bloom between 120°W and 180°W. The eastern and central equatorial region is different in that it is iron limited. Nutrients are supplied to the surface from equatorial upwelling, but the upwelled water does not have enough iron to support complete utilization of the nitrate [Barber and Chavez, 1991]. The well-known decrease/increase in equatorial

chlorophyll during El Niño/La Niña is shown here to be tied to the turning off and recommencement of the iron-rich EUC.

This study has focussed on SSH as an indicator of the thermocline depth; however, there are other physical processes that affect chlorophyll distributions, and not all of the observed chlorophyll changes can be explained simply by either changes in the thermocline or in the EUC. For example, in mode 1 the chlorophyll signal at the equator extends farther west than the SSH signal by ~20° longitude. This could be due to advection smearing out the chlorophyll signal, although it seems unlikely that advective effects would operate over such large scales. Equatorial chlorophyll changes are observed during the La Niña that are not associated with changes in the strength or depth of the EUC, and they could be related to other factors, such as the strength of local upwelling, temporal changes in the iron level of the EUC, or changes in grazing pressures on the phytoplankton.

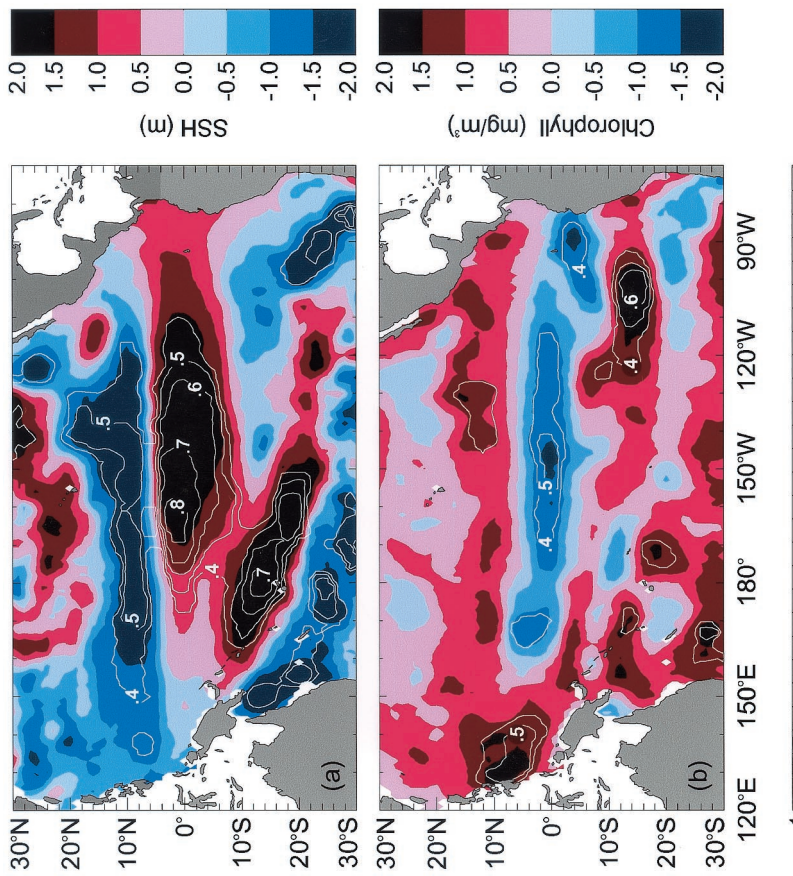
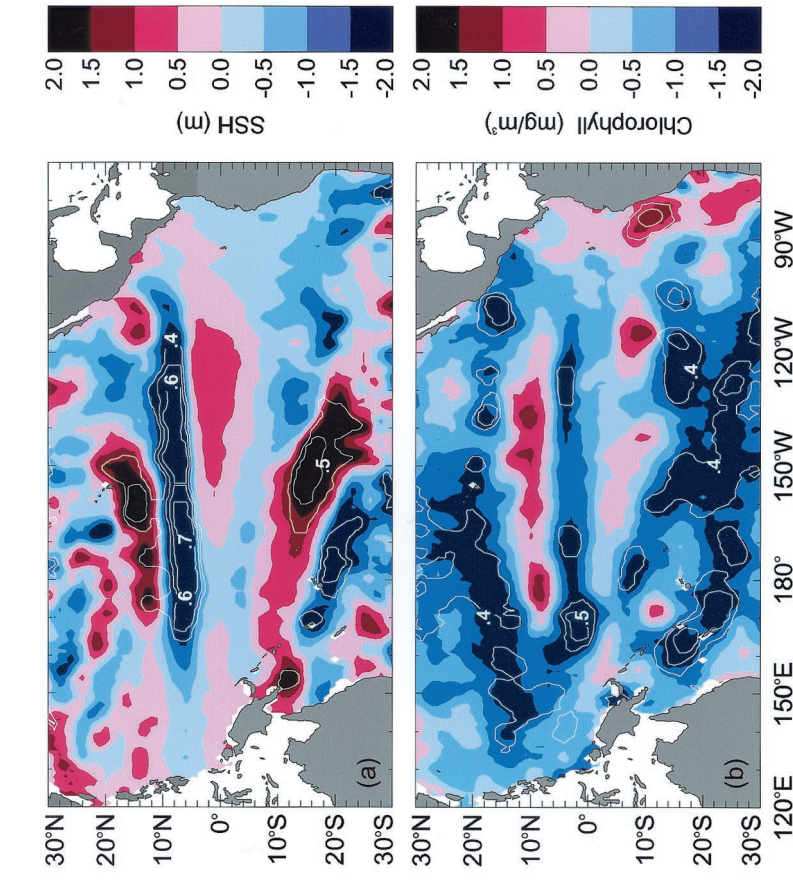


Plate 6. Same as in Plate 2 but for mode 2 of the joint EOF analysis of SSH and chlorophyll. Plate 6c shows the normalized principal component for the joint analysis (green), the normalized NINO3 index (black), and the normalized individual mode 2 SSH and chlorophyll principal components (dashed blue and dashed red lines, respectively). This mode accounts for 13% of the total variance.

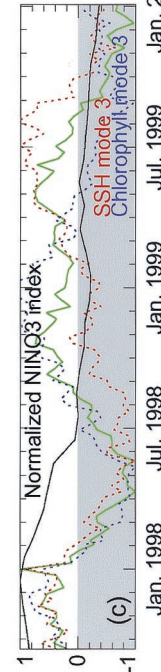


Plate 7. Same as in Plate 6 but for mode 3 of the joint EOF analysis of SSH and chlorophyll. This mode accounts for 8% of the total variance.

The temporal and spatial resolution of the TOPEX/Poseidon and SeaWiFS satellite data has allowed a basin-wide view of the biophysical coupling during the 1997–1998 ENSO event. The global correlations presented in Figure 2 suggest that there are basin-scale phenomena in the Indian Ocean that drive physical-biological covariability during the 1997–1998 ENSO event. This is not surprising, as Indian Ocean variability is often linked to western Pacific variability, especially during ENSO. However, away from the tropical Pacific and Indian Oceans, covariability between SSH and chlorophyll are lower, suggesting that other factors different from internal ocean dynamics may be responsible for the limiting factor of ocean productivity. Future studies will examine the role of surface forcings in chlorophyll variability in the extra-tropical Pacific as well as in other ocean basins.

Acknowledgments. We thank the SeaWiFS Project (Code 970.2) and the Distributed Active Archive Center (Code 902) at the NASA Goddard Space Flight Center for the production and distribution of the SeaWiFS data; the NASA Physical Oceanography Distributed Active Archive Center at the Jet Propulsion Laboratory, California Institute of Technology, for the TOPEX/Poseidon data; and the TAO Project Office and NOAA/PMEL/OCRD for the TAO/TRITON ADCP data. Additional thanks go to Victoria Coles for stimulating discussions and for the thermocline data and to Jim Yoder and an anonymous reviewer who gave valuable comments on an earlier draft of the manuscript.

References

- Adamec, D., Modulation of the seasonal signal of the Kuroshio Extension during 1994 from satellite data, *J. Geophys. Res.*, **103**, 10,209–10,222, 1998.
- Barale, V., C. McClain, and P. Malanotte-Rizzoli, Space and time variability of the surface color field in the northern Adriatic Sea, *J. Geophys. Res.*, **91**, 12,957–12,974, 1986.
- Barber, R., and F. Chavez, Regulation of primary productivity rate in the equatorial Pacific, *Limnol. Oceanogr.*, **36**, 1803–1815, 1991.
- Barber, R. T., M. P. Sanderson, S. T. Lindley, F. Chai, J. Newton, C. C. Trees, D. G. Foley, and F. P. Chavez, Primary productivity and its regulation in the equatorial Pacific during and following the 1991–1992 El Niño, *Deep Sea Res.*, **43**, 933–969, 1996.
- Bartolacci, D. M., and M. E. Luther, Patterns of co-variability between physical and biological parameters in the Arabian Sea, *Deep Sea Res.*, **46**, 1933–1964, 1999.
- Bidigare, R. R., and M. E. Ondrusek, Spatial and temporal variability of phytoplankton pigment distributions in the central equatorial Pacific Ocean, *Deep Sea Res.*, **43**, 809–833, 1996.
- Bretherton, F. B., R. E. Davis, and C. B. Fandry, A technique for objective analysis and design of oceanographic experiments applied to MODE-73, *Deep Sea Res.*, **23**, 559–582, 1976.
- Bretherton, C. S., C. Smith, and J. M. Wallace, An intercomparison of methods for finding coupled patterns in climate data, *J. Clim.*, **5**, 541–560, 1992.
- Chavez, F. P., P. G. Strutton, and M. J. McPhaden, Biological-physical coupling in the central equatorial Pacific during the onset of the 1997–98 El Niño, *Geophys. Res. Lett.*, **25**, 3543–3546, 1998.
- Chavez, F. P., P. G. Strutton, G. E. Friederich, R. A. Feely, G. C. Feldman, D. G. Foley, and M. J. McPhaden, Biological and chemical response of the equatorial Pacific to the 1997–98 El Niño, *Science*, **286**, 2126–2131, 1999.
- Chelton, D. B., and R. E. Davis, Monthly mean sea level variability along the west coast of North America, *J. Phys. Oceanogr.*, **6**, 757–784, 1982.
- Coale, K., S. Fitzwater, R. M. Gordon, K. Johnson, and R. Barber, Control of community growth and export production by upwelled iron in the equatorial Pacific Ocean, *Nature*, **379**, 621–624, 1996.
- Dandonneau, Y., Monitoring the sea surface chlorophyll concentrations in the tropical Pacific: Consequences of the 1982–83 El Niño, *Fish. Bull.*, **84**, 687–695, 1986.
- Dandonneau, Y., and F. Gohin, Meridional and seasonal variations of the sea surface chlorophyll concentration in the southwestern tropical Pacific (14 to 32°S, 160 to 175°E), *Deep Sea Res.*, **31**, 1377–1393, 1984.
- Davis, R. E., Predictability of sea surface temperature and sea level pressure anomalies over the North Pacific Ocean, *J. Phys. Oceanogr.*, **6**, 249–266, 1976.
- Dymond, J., and R. Collier, Biogenic particle fluxes in the equatorial Pacific: Evidence for both high and low productivity during the 1982–1983 El Niño, *Global Biogeochem. Cycles*, **2**, 129–137, 1988.
- Emery, W. J., and R. E. Thomson, *Data Analysis Methods in Physical Oceanography*, Pergamon, New York, 1997.
- Feldman, G., D. Clark, and D. Halpern, Satellite color observations of the phytoplankton distribution in the eastern equatorial Pacific during the 1982–1983 El Niño, *Science*, **226**, 1069–1071, 1984.
- Fiedler, P. C., F. P. Chavez, D. W. Behringer, and S. B. Reilly, Physical and biological effects of Los Niños in the eastern tropical Pacific, 1986–1989, *Deep Sea Res.*, **39**, 199–219, 1992.
- Friedrichs, M., and E. Hofmann, Physical control of biological processes in the central equatorial Pacific Ocean, *Deep Sea Res.*, **48**, 1023–1069, 2001.
- Frost, B. W., and N. C. Franzen, Grazing and iron limitation in the control of phytoplankton stock and nutrient concentration: A chemostat analogue of the Pacific equatorial upwelling system, *Mar. Ecol. Prog. Ser.*, **83**, 291–303, 1992.
- Gordon, R., K. Coale, and K. Johnson, Iron distributions in the equatorial Pacific: Implications for new production, *Limnol. Oceanogr.*, **42**, 419–431, 1997.
- Halpern, D., and G. C. Feldman, Annual and interannual variations of phytoplankton pigment concentration and upwelling along the Pacific equator, *J. Geophys. Res.*, **99**, 7347–7354, 1994.
- Hooker, S., and C. McClain, The calibration and validation of SeaWiFS data, *Prog. Oceanogr.*, **45**, 427–465, 2000.
- Johnson, G. C., and M. J. McPhaden, Interior pycnocline flow from the subtropical to the equatorial Pacific Ocean, *J. Phys. Oceanogr.*, **29**, 3073–3089, 1999.
- Johnson, G. C., M. J. McPhaden, G. D. Rowe, and K. E. McTaggart, Upper equatorial Pacific Ocean current and salinity variability during the 1996–1998 El Niño–La Niña cycle, *J. Geophys. Res.*, **105**, 1037–1053, 2000.
- Karl, D., R. Letelier, D. Hebel, L. Tupas, J. Dore, J. Christian, and C. Winn, Ecosystem changes in the North Pacific subtropical gyre attributed to the 1991–1992 El Niño, *Nature*, **373**, 230–233, 1995.
- Kessler, W. S., and B. A. Taft, Dynamic heights and zonal geostrophic transports in the central tropical Pacific during 1979 to 1984, *J. Phys. Oceanogr.*, **17**, 97–122, 1987.
- Kutzbach, J., Empirical eigenvectors of sea-level pressure, surface temperatures and precipitation complexes over North America, *J. Appl. Meteorol.*, **6**, 791–802, 1967.
- Landry, M. R., et al., Iron and grazing constraints on primary production in the central equatorial Pacific, *Limnol. Oceanogr.*, **42**, 405–418, 1997.
- Leonard, C. L., and C. R. McClain, Assessment of interannual variation (1979–1986) in pigment concentrations in the tropical Pacific using the CZCS, *Int. J. Remote Sens.*, **17**, 721–732, 1996.
- Levitus, S., and T. P. Boyer, *World Ocean Atlas 1994*, vol. 4, *Temperature*, NOAA Atlas NESDIS 4, Natl. Oceanic and Atmos. Admin., Silver Spring, Md., 1994.
- Levitus, S., R. Burgett, and T. P. Boyer, *World Ocean Atlas 1994*, vol. 3, *Salinity*, NOAA Atlas NESDIS 3, Natl. Oceanic and Atmos. Admin., Silver Spring, Md., 1994.
- Mackey, D. J., J. S. Parslow, F. B. Griffiths, H. W. Higgins, and B. Tilbrook, Plankton productivity and the carbon cycle in the western equatorial Pacific under El Niño and non-El Niño conditions, *Deep Sea Res.*, **44**, 1951–1978, 1997.
- Mariano, A. J., G. L. Hitchcock, C. J. Ashjian, D. B. Olsen, T. Rossby, E. Ryan, and S. L. Smith, Principal component analysis of biological and physical variability in a Gulf Stream meander crest, *Deep Sea Res.*, **43**, 1531–1565, 1996.
- Martin, J. H., R. M. Gordon, and S. Fitzwater, The case for iron, *Limnol. Oceanogr.*, **36**, 1793–1800, 1991.
- McPhaden, M. J., Genesis and evolution of the 1997–98 El Niño, *Science*, **283**, 950–954, 1999.
- McPhaden, M. J., et al., The Tropical Ocean–Global Atmosphere observing system: A decade of progress, *J. Geophys. Res.*, **103**, 14,169–14,240, 1998.
- Murakami, H., J. Ishizaka, and H. Kawamura, ADEOS observations of chlorophyll *a* concentration, sea surface temperature, and wind

- stress change in the equatorial Pacific during the 1997 El Niño onset, *J. Geophys. Res.*, **105**, 19,551–19,559, 2000.
- Murtugudde, R., S. Signorini, J. Christian, A. Busalacchi, C. R. McClain, and J. Picaut, Ocean color variability of the tropical Indo-Pacific basin observed by SeaWiFS during 1997–1998, *J. Geophys. Res.*, **104**, 18,351–18,366, 1999.
- North, G. R., T. L. Bell, R. F. Cahalan, and F. J. Moeng, Sampling errors in the estimation of empirical orthogonal functions, *Mon. Weather Rev.*, **111**, 699–706, 1982.
- Philander, S. G., *El Niño, La Niña and the Southern Oscillation*, Academic, San Diego, Calif., 1990.
- Polovina, J., G. Mitchum, and G. T. Evans, Decadal and basin-scale variation in mixed layer depth and the impact on biological production in the central and North Pacific, 1960–1988, *Deep Sea Res.*, **42**, 1701–1716, 1995.
- Preisendorfer, R. W., *Principal Component Analysis in Meteorology and Oceanography*, Elsevier Sci., New York, 1988.
- Signorini, S., C. R. McClain, and Y. Dandonneau, Mixing and phytoplankton bloom in the wake of the Marquesas Islands, *Geophys. Res. Lett.*, **26**, 3121–3124, 1999.
- Taft, B. A., and W. S. Kessler, Variations of zonal currents in the central tropical Pacific during 1970 to 1987: Sea level and dynamic height measurements, *J. Geophys. Res.*, **96**, 12,599–12,618, 1991.
- Trenberth, K. E., The definition of El Niño, *Bull. Am. Meteorol. Soc.*, **78**, 2771–2777, 1997.
- Vincent, D. G., The South Pacific Convergence Zone (SPCZ): A review, *Mon. Weather Rev.*, **122**, 1949–1970, 1994.
- Wyrtki, K., The response of sea surface topography to the 1976 El Niño, *J. Phys. Oceanogr.*, **9**, 1223–1231, 1979.

D. Adamec, NASA Goddard Space Flight Center, Oceans and Ice Branch, Code 971, Greenbelt, MD 20771, USA.
(adamec@gsfc.nasa.gov)

C. Wilson, NASA Goddard Space Flight Center, GEST Center, Code 971, Greenbelt, MD 20771, USA. (cara.wilson@gsfc.nasa.gov)

(Received November 20, 2000; revised July 30, 2001;
accepted July 30, 2001.)